Normalized iterative denoising ghost imaging based on the adaptive threshold

2017 Laser Phys. Lett. 14 025207

(http://iopscience.iop.org/1612-202X/14/2/025207)

IOP Publishing | Astro Ltd
Laser Physics Letters
Laser Phys. Lett. **14** (2017) 025207 (6pp)
doi:10.1088/1612-202X/aa555e

Letter

Normalized iterative denoising ghost imaging based on the adaptive threshold

Gaoliang Li, Zhaohua Yang, Yan Zhao, Ruitao Yan, Xia Liu and Baolei Liu

School of Instrumentation Science and Opto-electronics Engineering, Beihang University, Beijing, People's Republic of China

E-mail: yangzh@buaa.edu.cn

Received 24 November 2016, revised 12 December 2016
Accepted for publication 21 December 2016
Published 10 January 2017

Abstract

An approach for improving ghost imaging (GI) quality is proposed. In this paper, an iteration model based on normalized GI is built through theoretical analysis. An adaptive threshold value is selected in the iteration model. The initial value of the iteration model is estimated as a step to remove the correlated noise. The simulation and experimental results reveal that the proposed strategy reconstructs a better image than traditional and normalized GI, without adding complexity. The NIDGI-AT scheme does not require prior information regarding the object, and can also choose the threshold adaptively. More importantly, the signal-to-noise ratio (SNR) of the reconstructed image is greatly improved. Therefore, this methodology represents another step towards practical real-world applications.

Keywords: ghost imaging, adaptive threshold, normalizing, iterative denoising

(Some figures may appear in colour only in the online journal)

1. Introduction

In recent years, researchers in the fields of quantum imaging [1–5] and classical optical imaging have paid more attention to ghost imaging (GI) [6–15] because of its high resolution, anti-jamming and high sensitivity for very weak signal. With the advantage of needing one bucket detector (BD) without spatial resolving power, GI has significant potential applicative value in remote sensing, medical treatment and microscopic imaging. At present, researchers are working to move GI from experimental evaluation towards real-world applications. However, the low signal-to-noise ratio (SNR) of GI algorithms based on thermal light (pseudo-thermal light) make it difficult to meet application requirements. Thus, improving the image quality of GI is one of the key problems that must be solved.

In order to solve this problem, many scholars have researched related areas extensively. For example, an algorithm called normalized ghost imaging (NGI) is proposed in [9], and this has a more appropriate weighting factor applied to the ensemble average of the estimated object. This algorithm shows a remarkable enhancement compared to the traditional GI algorithm [6]. On the basis of correspondence ghost imaging (CGI) [10–12], proposed by Luo *et al*, this method has been enhanced as positive–negative correspondence ghost imaging (P–NCGI) [13, 14] and double-threshold time correspondence imaging (DTTCI) [15]. Although the reconstructed image quality is far better than for GI, it is not comparable with the imaging quality of normalized correlation imaging. Compressive sensing (CS) [16] and adaptive compressive ghost imaging (ACGI) [17–19] have the merit of high resolution. However, a more complex image with expensive memory requirements can lead to computation times of tens of minutes or longer. Iterative denoising of ghost imaging (IDGI) [20–22] shows much better performance than differential ghost imaging (DGI) [23] through estimating the noise via the conventional GI algorithm, without considering the universal practicality of the threshold selection [20]. Following the above cases, the aim of this paper is to propose an innovative method for improving the SNR value using an iterative algorithm based on NGI, without requiring the introduction of other GI methods for noise estimation.

Normalized iterative denoising ghost imaging based on the adaptive threshold (NIDGI-AT) is proposed to remove the noise based on NGI. Firstly, we theoretically analyze why the SNR of NGI is higher than GI, and build an iteration model based on NGI from the point of view of removing the noise. Secondly, the initial value of the iteration model is estimated as a step towards removing the correlated noise, and the optimum factor of the correlated noise is obtained through simulation experiments. Finally, the iterative selection method for the adaptive threshold based on normalized iterative denoising GI is designed. It is shown that it can improve the quality of the reconstructed image effectively compared with NGI and resist the influence of background noise at the same time.

2. Theoretical scheme and simulation

The experimental setup, shown in figure 1, is a GI system. The pseudo-thermal light is separated by a beam splitter (BS) into two correlated arms. In the signal arm, the light goes through an Obj (object) and the total intensity is collected by the BD. In the reference arm, the light intensity distribution is received by the charge-coupled device (CCD) detector. Then the target image is obtained via the second-order correlation operation [24] of two optical signals. In GI, the traditional second-order correlation fluctuation function can be written as [25, 26]

$$\Delta G^{(2)}(x) = \langle I_{\mathrm{B}} I_{\mathrm{R}}(x)\rangle - \langle I_{\mathrm{B}}\rangle\langle I_{\mathrm{R}}(x)\rangle, \tag{1}$$

where $I_{\mathrm{R}}^{(i)}(x)$ is the reference detection value, x is the transverse spatial coordinate and the bucket detection is recorded as $I_{\mathrm{B}}^{(i)} = \sum_x I_{\mathrm{R}}^{(i)}(x)T(x)$, and $i=1, 2, 3\cdots$. $T(x)$ denotes the intensity transmission function of the object. K represents the total number of measurements. The covariance of the x and x' points in the light field is defined as

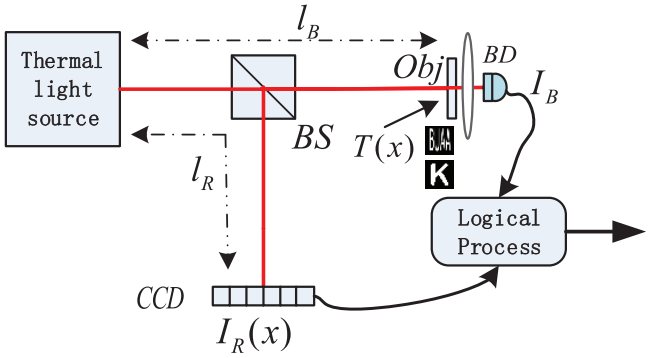

Figure 1. Schematic of the experimental setup.

$$\sigma^2(x,x') = \frac{1}{K}\sum_{i=1}^{K} I_R^{(i)}(x) I_R^{(i)}(x') - \frac{1}{K}\sum_{i=1}^{K} I_R^{(i)}(x)\frac{1}{K}\sum_{i=1}^{K} I_R^{(i)}(x'). \tag{2}$$

Equation (1) can be expressed as

$$\begin{aligned}\Delta G^{(2)}(x) &= \frac{1}{K}\sum_{i=1}^{K} I_{\mathrm{B}}^{(i)} I_{\mathrm{R}}^{(i)}(x) - \frac{1}{K}\sum_{i=1}^{K} I_{\mathrm{B}}^{(i)}\frac{1}{K}\sum_{i=1}^{K} I_{\mathrm{R}}^{(i)}(x)\\ &= \frac{1}{K}\sum_{i=1}^{K}\left(\sum_{x'} I_{\mathrm{R}}^{(i)}(x')T(x')\right) I_{\mathrm{R}}^{(i)}(x)\\ &\quad - \frac{1}{K}\sum_{i=1}^{K}\sum_{x'} I_{\mathrm{R}}^{(i)}(x')T(x')\frac{1}{K}\sum_{i=1}^{K} I_{\mathrm{R}}^{(i)}(x)\\ &= \sigma^2\left(\sum_{x'} I_{\mathrm{R}}^{(i)}(x')T(x'), I_{\mathrm{R}}^{(i)}(x)\right)\\ &= \sum_{x\neq x'} T(x')\sigma^2(x',x) + T(x)\sigma^2(x,x).\end{aligned} \tag{3}$$

Two papers [9, 10] showed that NGI improves image quality greatly compared to traditional GI. Combined with equation (3), we can obtain another form of NGI

$$\begin{aligned}G_{\mathrm{NGI}}^{(2)}(x) &= \frac{1}{\bar{S}_{\mathrm{R}}}\frac{1}{K}\sum_{i=1}^{K} I_{\mathrm{B}}^{(i)} I_{\mathrm{R}}^{(i)}(x) - \frac{1}{\bar{S}_{\mathrm{R}}{}^2}\frac{1}{K}\sum_{i=1}^{K} I_{\mathrm{B}}^{(i)}\frac{1}{K}\sum_{i=1}^{K}\left(I_{\mathrm{R}}^{(i)}(x)\sum_{x}^{N} I_{\mathrm{R}}^{(i)}(x)\right)\\ &= \frac{1}{\bar{S}_{\mathrm{R}}}\frac{1}{K}\sum_{i=1}^{K} I_{\mathrm{B}}^{(i)} I_{\mathrm{R}}^{(i)}(x) - \frac{1}{\bar{S}_{\mathrm{R}}}\frac{1}{K}\sum_{i=1}^{K} I_{\mathrm{B}}^{(i)}\frac{1}{K}\sum_{i=1}^{K} I_{\mathrm{R}}^{(i)}(x) - \frac{1}{\bar{S}_{\mathrm{R}}{}^2}\frac{1}{K}\sum_{i=1}^{K} I_{\mathrm{B}}^{(i)}\frac{1}{K}\sum_{i=1}^{K}\left(I_{\mathrm{R}}^{(i)}(x)\sum_{x}^{N} I_{\mathrm{R}}^{(i)}(x)\right) + \frac{1}{\bar{S}_{\mathrm{R}}}\frac{1}{K}\sum_{i=1}^{K} I_{\mathrm{B}}^{(i)}\frac{1}{K}\sum_{i=1}^{K} I_{\mathrm{R}}^{(i)}(x)\\ &= \frac{1}{\bar{S}_{\mathrm{R}}}\left(\frac{1}{K}\sum_{i=1}^{K} I_{\mathrm{B}}^{(i)} I_{\mathrm{R}}^{(i)}(x) - \frac{1}{K}\sum_{i=1}^{K} I_{\mathrm{B}}^{(i)}\frac{1}{K}\sum_{i=1}^{K} I_{\mathrm{R}}^{(i)}(x) - \mu\left(\frac{1}{K}\sum_{i=1}^{K}\left(I_{\mathrm{R}}^{(i)}(x)\sum_{x}^{N} I_{\mathrm{R}}^{(i)}(x)\right) - \frac{1}{K}\sum_{i=1}^{K} I_{\mathrm{R}}^{(i)}(x)\frac{1}{K}\sum_{i=1}^{K}\sum_{x}^{N} I_{\mathrm{R}}^{(i)}(x)\right)\right),\end{aligned} \tag{4}$$

where $\bar{S}_{\mathrm{R}} = \frac{1}{K}\sum_{i=1}^{K}\sum_{x}^{N} I_{\mathrm{R}}^{(i)}(x)$, and $\mu = \frac{1}{K}\sum_{i=1}^{K} I_{\mathrm{B}}^{(i)} / \frac{1}{K}\sum_{i=1}^{K}\sum_{x}^{N} I_{\mathrm{R}}^{(i)}(x)$.

From equations (3) and (4) we can obtain

$$\begin{aligned}G_{\mathrm{NGI}}^{(2)}(x) &= \frac{1}{\bar{S}_{\mathrm{R}}} T(x)\sigma^2(x,x) + \frac{1}{\bar{S}_{\mathrm{R}}}\sum_{x\neq x'}\sigma^2(x,x')T(x')\\ &\quad - \mu\frac{1}{\bar{S}_{\mathrm{R}}}\sum_{x'}\sigma^2(x,x'),\end{aligned} \tag{5}$$

and $T' = \frac{1}{K}\sum_{i=1}^{K} I_{\mathrm{B}}^{(i)}/\bar{S}_{\mathrm{R}}$, where $\sigma^2(x,x)$ is the autocorrelation coefficient. At present, the methods used to remove noise in GI concentrate on analyzing the optical system and the modulation of the light field. From the viewpoint of NGI, we analyze the internal noise sources and study effective methods for removing the background noise. Equation (5) shows that every pixel of the image can be divided into three parts from the viewpoint of denoising: $\frac{1}{\bar{S}_{\mathrm{R}}} T(x)\sigma^2(x,x)$ is the real image without noise in the GI of a pseudo-thermal light source.

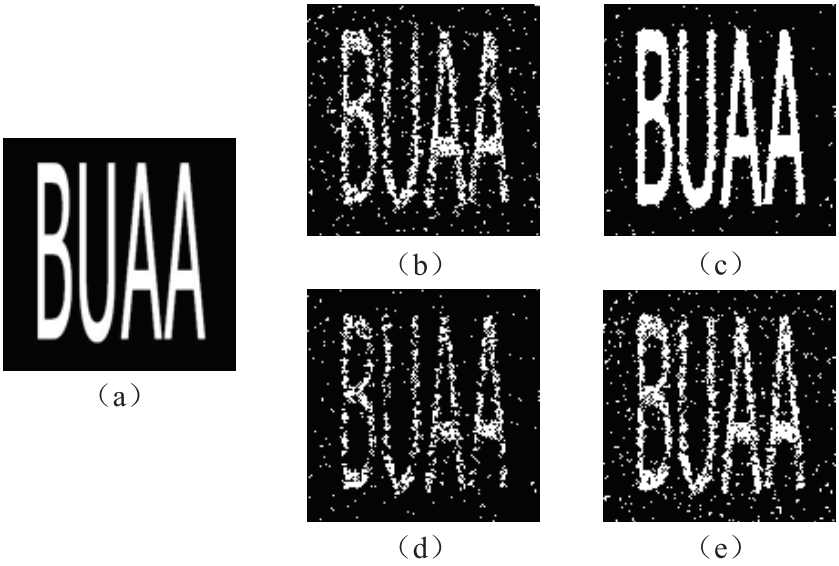

Figure 2. Reconstructed images of several typical t values from $c = 0.46$. (a) Digital mask of 'BUAA', (b) image retrieved with $t = 100$, (c) image retrieved with $t = 300$, (d) image retrieved with $t = 600$ and (e) image retrieved with $t = 800$.

Table 1. SNR for different t values.

t	100	200	300	400	500	600	700	800	900
SNR	1.45	1.42	4.72	1.36	1.51	1.26	1.42	1.53	1.37

$\frac{1}{\overline{S}_R}\sum_{x\neq x'}\sigma^2(x,x')T(x')$, which comes from coherent light sources and a limited number of measurements, can be understood as the background noise of the system. $\mu\frac{1}{\overline{S}_R}\sum_{x'}\sigma^2(x,x')$ shows part of the background noise removed by NGI, and this is also the reason that the imaging quality of NGI is superior to that of traditional GI.

However, in equation (5), the middle and third parts are not absolutely equal, and thus the background noise is not completely removed; the residual noise is expressed as e. This background noise is also found in experiments. So, an iterative denoising model is established to obtain a better quality reconstructed image based on NGI by removing the residual noise e, and the model is expressed as

$$\mathrm{INGI}^{(j+1)}(x) = \frac{1}{\overline{S}_R}T(x)\sigma^2(x,x) + \frac{1}{\overline{S}_R}\sum_{x\neq x'}\sigma^2(x,x')T(x') - c\mathrm{INGI}^{(j)}(x), \tag{6}$$

where $T(x')$ is the retrieved NGI image, and $c\mathrm{INGI}^{(j)}$is the noise we expect to be suppressed, which can be expressed as $c\mathrm{INGI}^{(j)}(x) = \frac{1}{\overline{S}_R}T'\sum_{x\neq x'}\sigma^2(x,x') + e$. The removed noise in NGI is $1/\overline{S}_R T'\sum_{x\neq x'}\sigma^2(x,x')$. The noise estimated from the iterative denoising model is represented by e.

The model for removing noise has been given, and then the initial value should be estimated—according to the definition of NGI [9], we deduce that

$$G^{(2)}_{\mathrm{NGI}}(x)_K = \frac{1}{K}\sum_{i=1}^{K}O_i(x) = \frac{K-1}{K}G^{(2)}_{\mathrm{NGI}}(x)_{K-1} + \frac{1}{K}O_K(x). \tag{7}$$

To implement NGI, which can dramatically enhance the SNR, we need to define the value of x in the number i measurement $O_i(x) = S_N^{(i)}\delta I_R^{(i)}(x)$. The differential bucket signal can be written in an operative form as $S_N^{(i)} = I_B^{(i)}/S_R^{(i)} - \langle I_B\rangle_{(i)}/\langle S_R\rangle_{(i)}$, and the value of the reference arm signal is $\delta I_R^{(i)}(x) = I_R^{(i)}(x) - \langle I_R(x)\rangle_{(i)}$.

When K is large enough (such as 10^4), both theoretical analysis and experimental results show that its value changes little, for example increasing or decreasing by 1, so it has little effect on the result. Hence it is difficult to estimate the noise of the image. Then, from equations (6) and (7) we can obtain

$$G^{(2)}_{\mathrm{NGI}}(x)_K = \frac{K-t}{K}G^{(2)}_{\mathrm{NGI}}(x)_{K-t} + \frac{1}{K}\sum_{i=K-t+1}^{K}O_i(x) = \frac{K-t}{K}G^{(2)}_{\mathrm{NGI}}(x)_{K-t} + \frac{1}{K}\sum_{i=K-t+1}^{K}O'_i(x) + e_t, \tag{8}$$

where t is a factor of the correlated noise of t and e_t is the correlated noise of the reconstructed image with t. The K value is generally of the order of magnitude of 10^4. Choosing a t that is too small results in the image being fuzzy, and too large a t leads to poor noise removal. So, we obtain the range of t ($100 \leqslant t \leqslant 900$) according to the experience of the simulation data. It is clear that t is much smaller than K, and the normalized value is relatively small, too. Therefore, we think that $1/K\sum_{i=K-t+1}^{K}O'_i(x)$ is close to 0, and then the equation (8) can be converted into

$$G^{(2)}_{\mathrm{NGI}}(x)_K = \frac{K-t}{K}G^{(2)}_{\mathrm{NGI}}(x)_{K-t} + e_t. \tag{9}$$

So, the normalized iterative denoising GI model can be obtained from equations (6) and (9)

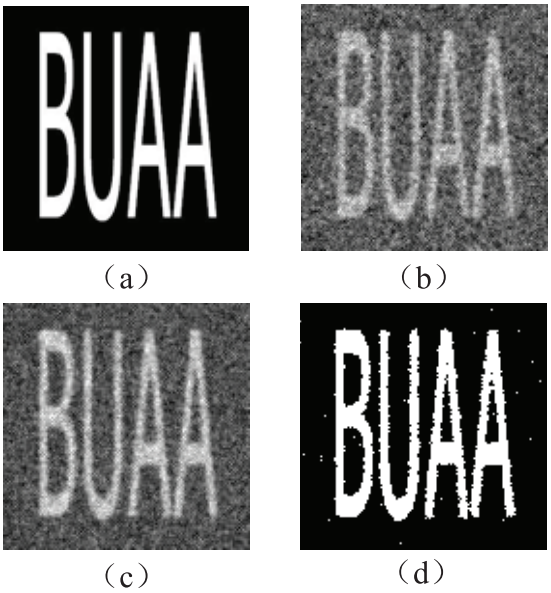

Figure 3. Simulated results for fluctuation GI, NGI and NIDGI-AT, with 20 000 measurements. (a) Digital mask of 'BUAA'; (b) fluctuation GI image, with SNR = 1.44; (c) NGI image, with SNR = 1.91; and (d) NIDGI-AT image in the case where $c = 0.56$, with SNR = 5.93.

$$\begin{cases} \mathrm{INGI}^{(j)}(x) = G^{(2)}_{\mathrm{NGI}}(x)_K - \dfrac{K-t}{K} G^{(2)}_{\mathrm{NGI}}(x)_{K-t} \quad (j=1) \\ \mathrm{INGI}^{(j)}(x) = \dfrac{1}{\bar{S}_{\mathrm{R}}} T(x)\sigma^2(x,x) + \dfrac{1}{\bar{S}_{\mathrm{R}}} \sum_{x \neq x'} \sigma^2(x,x')T(x'), \\ \qquad -c\mathrm{INGI}^{(j-1)}(x) \quad (j=2,3,4...) \end{cases} \tag{10}$$

where j is the number of iterations of the NIDGI-AT scheme. Through experiments, it is found that the SNR of NIDGI-AT reaches optimality when $j = 3$. This j value will be used in the simulations and experiments in this paper. To obtain a better value of t for the estimation of the correlated noise, a computational experiment is performed. First of all, the SNR of the retrieved image is defined as [27–29]

$$\mathrm{SNR} = \frac{\sum_{r,c=1}^{m,n} (U_0(r,c) - T)^2}{\sum_{r,c=1}^{m,n} (U(r,c) - U_0(r,c))^2}, \tag{11}$$

where m, n represent the array of an object of size $m \times n$ pixels, $U(r, c)$ and $U_0(r, c)$ denote the gray tone of the (r, c)th pixel of the target object and the reconstructed image, respectively, and $T = {}^{1}/_{m \times n} \sum U_0(r,c)$ is the average gray tone of the object. As shown in figure 2, in the case of a random selection of a threshold c, a few typical t values corresponding to the image are reconstructed using the normalized iterative denoising GI method. We can see that when the t takes different values, the image quality is obviously different. Figure 2(a) illustrates the original. Figures 2(b)–(e) are the image effects of $t = 100$, 300, 600 and 800, respectively. It is obvious that figure 2(c) is better than the others, so a suitable t value directly affects the quality of the reconstructed image.

Figure 2 indicates the results for the qualitative comparison of typical images. In order to obtain the best t value, we also

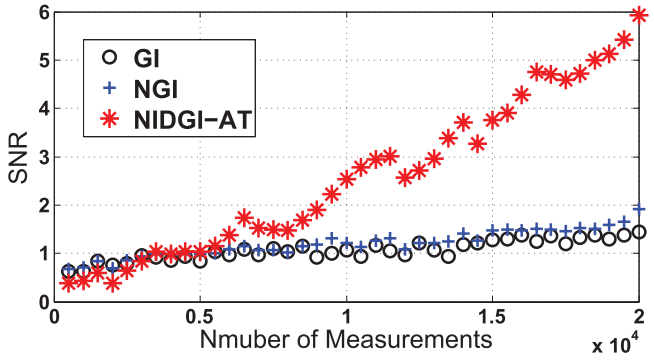

Figure 4. The SNR of fluctuation GI, NGI and NIDGI-AT for different numbers of measurements.

study the corresponding SNR values for different t values quantitatively. Table 1 demonstrates the corresponding distribution of different SNR values when t is between 100 and 900 for the conditions $K = 20\,000$ and $c = 0.46$. As can be seen from the quantitative SNR, the image quality is optimal when $t = 300$ when normalized iterative denoising GI is being used, while the SNR of the image reaches 4.72. Therefore, the value of t is set to 300 in the next simulation experiment.

The threshold c is one of the important parameters in NIDGI-AT, as shown in equation (10). Setting the threshold randomly is obviously unreasonable. Whether the threshold is too large or too small, the quality of the reconstructed image will be reduced. Furthermore, a reconstructed image with an inappropriate threshold cannot be implemented for an engineering application. Therefore, an adaptive threshold selection method based on iteration is designed in this paper [30]. Next, we discuss the iteration process for the adaptive threshold. Firstly, an initialization parameter is required. The initialization threshold c ($0 \leqslant c \leqslant 1$) is 0, the imaging system measurement number is K, the first-level iteration step threshold is 0.1 and the second-level iterative step threshold is 0.02. We set the input SNR value Q according to the actual engineering application from the sample. Secondly, we begin the first-level iteration ($c1 = c + 0.1$) using the normalized iterative denoising GI scheme. If the SNR value q from the NIDGI scheme is greater than Q, then the program ends and outputs the reconstructed image. If $Q - q < 0.5$, then we enter the second-level iteration, the iterative step threshold ($c2 = c1 - 0.02$) based on the first-level iteration. Otherwise, it enters the next program of the first-level iterative. Thirdly, when the program enters the second-level iteration, we repeat step 2. The program will terminate if $Q - q < 0.5$ is true. So the selection of the adaptive threshold can be realized. The SNR will be relatively large when the threshold c is within the 0.40–0.60 range from the simulation of the digital mask image 'BUAA'. So the first-level iteration threshold c is from 0.40 to 0.60. The imaging time is decreased by reducing the range of the threshold selection based on the training sample in the engineering application. Of course, if the SNR of image still does not reach the target value when the selections of the adaptive threshold is finished, we need to increase the number of measurements appropriately, and then repeat the processes described above.

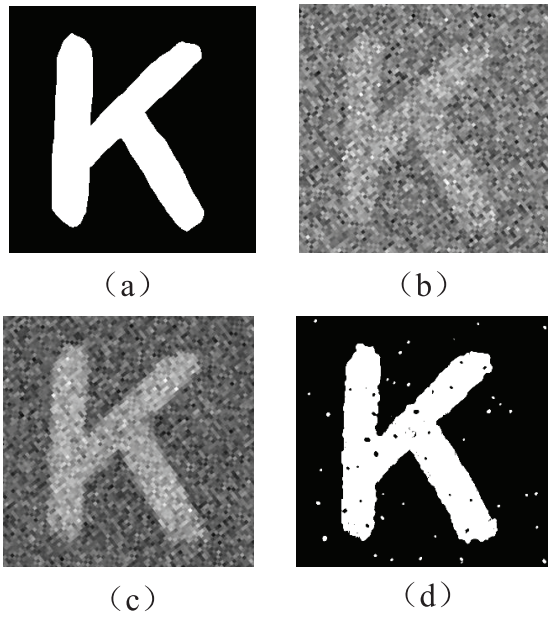

Figure 5. Experimental results for 20 000 measurements. (a) The original image; (b) fluctuation GI image, with SNR = 0.95; (c) NGI image, with SNR = 2.19; and (d) NIDGI-AT image for $c = 0.5$, with SNR = 6.28.

For the purpose of illustrating the simulation results for the NIDGI-AT scheme, we adopted various schemes of GI for image quality comparison. Figure 3(a) is the original mask image, and figures 3(b)–(d) show the image effect through fluctuation GI, NGI and NIDGI-AT reconstruction, respectively, under the conditions of 20 000 × measurement. To unify the quantification to compare the image quality of different algorithms, all the images are normalized to [0, 1]. The speckle is produced artificially in the simulation, which is consistent with a negative exponential probability distribution. The average speckle size is about 1 pixel size and the number of measurements K is equal to 20 000. The improvement of image quality in figure 3(b) compared with figure 3(c) proves that NGI obtains a higher SNR than traditional GI. The SNR in figure 3(d) reaches 5.93, which is better than that in figure 3(c). This is mainly because the correlated noises and background noise of the image are removed by the scheme of this paper.

In order to further study the contrast of the SNR from different measurements, the variation of the SNR of 40 points to the total number of measurements is shown in figure 4. Figure 4 indicates an increasing trend of the SNR corresponding to fluctuation GI, NGI and NIDGI-AT. The SNR of the NIDGI-AT scheme grows fastest, reflecting the advantage of the scheme proposed in this paper once again. However, it is not difficult to see that the SNR of NGI is slightly higher than that of NIDGI-AT when the measurement times are between 0 and 5000. Here we consider that these three schemes have a comparative reconstruction effect, mainly because the number of measurements is too small to judge the performance of the program. Compared with the other two methods, the SNR of the new scheme in this paper increases significantly when there are more than 5000 measurements.

3. Experimental results

The experimental setup, shown in figure 1, is a GI system. A linearly polarized 632 nm He–Ne laser beam is projected onto a ground-glass disk rotating at 3 rad min^{-1} to produce a field of randomly varying speckles. This pseudo-thermal light is then separated by a BS into two correlated arms. In the reference arm, the light goes directly to the detector of the CCD cameras (Imaging Source VC-2MC-M340E0), whose active image pixels are 2048(H) ∗ 1088(V). We select the region of the 300(H) ∗ 300(V) pixel as the reference signal from the CCD. In the signal arm, the light goes through an Obj, and the total intensity is collected by the BD. The BD is replaced by a CCD camera of the same type, but it needs to be summed in the correlation computation. The distance from the beams to the object, and from the beams to the reference detector, is represented as l_B and l_R, respectively. Here $l_B = l_R = 245$ mm. The letter K is used as a digital mask with an actual size of 5 mm ∗ 5 mm. The computer used for the image reconstruction is a Lenovo desktop machine (CPU: Intel Core i7-4700 dual core, 2.40 GHz, 4 GB). The total number of measurements is 20 000. Figure 5 illustrates the experimental results for different GI methods. Figure 5(a) is the original image of the digital mask. Figure 5(b) shows the image reconstructed using the fluctuation GI method. Figure 5(c) is the result reconstructed using NGI. Figure 5(d) demonstrates the NIDGI-AT image in the case where $c = 0.5$. The experimental results indicate that the SNR of this paper is increased to 6.28 compared with NGI.

4. Conclusion

In conclusion, we propose a scheme that may be called NIDGI-AT. A universal model of iterative denoising based on NGI is established by analysing the correlated calculation model. Meanwhile, the initial value of the iteration model is estimated and the optimum factor for correlated noise is obtained through the simulation experiments. The background and correlated noise are efficiently suppressed by the normalized iterative denoising GI method mentioned in this paper. Without increasing the complexity or having a preference for the object, it is shown that NIDGI-AT offers better performance than NGI. Adaptive threshold selection to remove noise is also implemented in this paper. Therefore, this method can further advance GI towards practical application. Combined with the advantages of super-resolution and anti-interference, GI with a high SNR has extraordinary potential application value in medical diagnosis and treatment, and industrial detection. Of course, we have only studied black-and-white mask images through simulation and experimentation in this paper. Whether grayscale images can be affected by normalized iterative denoising GI will be a topic of future research for us.

Acknowledgments

This work was supported in part by the Natural Science Foundation of China under grant 61233005 and 61473022, and the

National 973 Project under grant no. 2014CB744200. The authors also gratefully acknowledge the helpful comments and suggestions of the reviewers and editors.

References

[1] Brown R H and Twiss R Q 1994 Correlation between photons in two coherent beams of light *J. Astrophys. Astron.* **15** 13–26

[2] Pittman T B, Shih Y H, Strekalov D V and Sergienko A V 1995 Optical imaging by means of two-photon quantum entanglement *Phys. Rev.* A **52** R3429–32

[3] D'Angelo M and Shih Y H 2005 Quantum imaging *Laser Phys. Lett.* **2** 567–96

[4] Han S 2009 Quantum noise analysis in correlated two-photon imaging *J. Mod. Opt.* **56** 851–4

[5] Shapiro J H and Boyd R W 2012 The physics of ghost imaging *Quantum Inform. Process.* **11** 949–93

[6] Liu X F, Chen X H, Yao X R, Yu W K, Zhai G J and Wu L A 2014 Lensless ghost imaging with sunlight *Opt. Lett.* **39** 2314–7

[7] Low G H, Yoder T J and Chuang I L 2014 Quantum imaging by coherent enhancement *Phys. Rev. Lett.* **114** 100801

[8] Li M F, Mo X F, Zhao L J, Huo J, Yang R, Li K and Zhang A N 2016 Single-pixel remote imaging based on Walsh–Hadamard transform *Acta Phys. Sin.* **65** 064201

[9] Sun B Q, Welsh S S, Edgar M P, Shapiro J H and Padgett M J 2012 Normalized ghost imaging *Opt. Express* **20** 16892–901

[10] Gatti A, Brambilla E, Bache M and Lugiato L 2004 Correlated imaging, quantum and classical *Phys. Rev.* A **70** 013802

[11] Bennink R S, Bentley S J, Boyd R W and Howell J C 2004 Quantum and classical coincidence imaging *Phys. Rev. Lett.* **92** 033601

[12] Luo K H, Huang B, Zheng W M and Wu L A 2012 Nonlocal imaging by conditional averaging of random reference measurements *Chin. Phys. Lett.* **29** 74216–20

[13] Sun M J, Li M F and Wu L A 2015 Nonlocal imaging of a reflective object using positive and negative correlations *Appl. Opt.* **54** 7494–9

[14] Song S C, Sun M J and Wu L A 2016 Improving the signal-to-noise ratio of thermal ghost imaging based on positive–negative intensity correlation *Opt. Commun.* **366** 8–12

[15] Li M F, Zhang Y R, Liu X F, Yao X R, Luo K H, Fan H and Wu L A 2013 A double-threshold technique for fast time-correspondence imaging *Appl. Phys. Lett.* **103** 211114–9

[16] Katz O, Bromberg Y and Silberberg Y 2009 Compressive ghost imaging *Appl. Phys. Lett.* **95** 131110–3

[17] Yu W K, Li M F, Yao X R, Liu X F, Wu L A and Zhai G J 2014 Adaptive compressive ghost imaging based on wavelet trees and sparse representation *Opt. Express* **22** 7133–44

[18] Dai H, Gu G, He W, Liao F, Zhuang J, Liu X and Chen Q 2014 Adaptive compressed sampling based on extended wavelet trees *Appl. Opt.* **53** 6619–28

[19] Huo Y, He H and Chen F 2016 Compressive adaptive ghost imaging via sharing mechanism and fellow relationship *Appl. Opt.* **55** 3356–67

[20] Yao X R, Yu W K, Liu X F, Li L Z, Li M F, Wu L A and Zhai G J 2014 Iterative denoising of ghost imaging *Opt. Exp.* **22** 24268–75

[21] Wang W, Wang Y P, Li J, Yang X and Wu Y 2014 Iterative ghost imaging *Opt. Lett.* **39** 5150–3

[22] Zhang W L, Zhang W W, He R Q and Chen Q 2016 Iterative denoising ghost imaging based on local Hadamard modulation *Acta Opt. Sin.* **36** 0411001

[23] Ferri F, Magatti D, Lugiato L A and Gatti A 2010 Differential ghost imaging *Phys. Rev. Lett.* **104** 253603

[24] Felbinger T and Wilkens M 1999 Stochastic wave-function simulation of two-time correlation functions *J. Mod. Opt.* **46** 1401–20

[25] Zhang D, Zhai Y H, Wu L A and Chen X H 2005 Correlated two-photon imaging with true thermal light *Opt. Lett.* **30** 2354–6

[26] Gatti A, Bondani M, Lugiato L A, Paris M G and Fabre C 2007 Comment on 'Can two-photon correlation of chaotic light be considered as correlation of intensity fluctuations?' *Phys. Rev. Lett.* **98** 039301

[27] Firbank M J, Coulthard A, Harrison R M and Williams E D 1999 A comparison of two methods for measuring the signal to noise ratio on MR images *Phys. Med. Biol.* **44** 261–4

[28] Erkmen B I and Shapiro J H 2009 Signal-to-noise ratio of Gaussian-state ghost imaging *Phys. Rev.* A **79** 023833

[29] Brida G, Chekhova M V, Fornaro G A, Genovese M, Lopaeva E D and Berchera I R 2011 Systematic analysis of signal-to-noise ratio in bipartite ghost imaging with classical and quantum light *Phys. Rev.* A **83** 063807

[30] Li G L, Zhao Y, Yang Z H and Liu X 2016 Positive–negative corresponding normalized ghost imaging based on an adaptive threshold *Laser Phys. Lett.* **13** 115202